Chapter 6 The cosmic microwave background

In Chapter 1 you learned about a radiation field called the cosmic microwave background (CMB) that permeates the entire Universe. In this chapter we will explore the observable characteristics of the CMB in much more detail and you will learn what they reveal about cosmic evolution and the cosmological parameters of the Universe.

In the previous chapter you learned that cosmologists can use observations of distant stars, galaxies and supernovae to measure the expansion rate of the Universe and thereby constrain the values of the cosmological parameters. In this chapter and the next you will learn that precise measurements of the CMB provide cosmologists with another, largely complementary way to measure the properties of the Universe.

At the end of the next chapter you will see that by combining the constraints derived from supernova observations with those derived from the CMB, cosmologists can derive very precise constraints for the cosmological parameters.

Objectives

Working through this chapter will enable you to:

- describe and understand the physical processes that produced the cosmic microwave background (CMB)
- explain the detailed observational properties of the CMB
- compare the capabilities of different telescopes that can be used to observe the CMB from the Earth and from space
- describe the challenges associated with observing the CMB
- summarise the ways that cosmologists mathematically describe and statistically model the spatial and spectral properties of the CMB.

6.1 The surface of last scattering

The Universe was almost completely opaque to electromagnetic radiation for the first $\sim 370\,000$ years of its evolution. During this time, the temperature of the Universe was much higher than it is today and typical photon energies were much larger than the ionisation potential Q of hydrogen. Consequently, the baryonic content of the Universe was almost completely ionised. Photons could only propagate for short distances before encountering a free electron and undergoing Thomson scattering, and any hydrogen atoms that did *briefly* form were almost immediately reionised.

This situation persisted until cosmological expansion and redshift reduced enough photons' energies below Q, which allowed widespread and rapid formation of long-lived hydrogen and helium atoms. As the number of free electrons fell, so did the Thomson scattering rate. Very soon, most photons were able to stream freely through the Universe and most have continued to do so ever since. It is *these* photons, released during the short interval when the Universe first became transparent, that have propagated without interaction ever since and make up the CMB.

Later chapters describe in more detail the physics that governed particle interactions and the co-evolution of matter and radiation during the Universe's early history. A key concept that will be needed for *this* chapter is that the photons making up the CMB effectively encode information about the state of the Universe when it was less than half a million years old and looked very different from the way it does today.

The speed at which the Universe became transparent means that all of the photons that make up the CMB have travelled a very similar distance since the last time they underwent Thomson scattering. For this reason the CMB, as seen by a *particular* observer, is often described as having been emitted from a spherical **surface of last scattering**. The time in the Universe's history when a *typical* CMB photon last underwent Thomson scattering is called the **epoch of last scattering**, which we can abbreviate as $t_{\rm ls}$. We will also use the notation $z_{\rm ls}$ to represent the redshift measured today for photons that were emitted at $t_{\rm ls}$. The numerical value of $z_{\rm ls}$ is approximately 1090.

Observers at different locations in the Universe detect CMB photons from *different* surfaces of last scattering. Figure 6.1 shows that all such surfaces have the same proper radius, which we denote using the symbol $d_{\rm p}(t_0, z_{\rm ls})$. This notation represents the proper distance measured at the present time, t_0, travelled by photons with observed redshift $z_{\rm ls}$. Note that the surface of last scattering is closer than the present-day horizon distance $d_{\rm hor}(t_0)$, so we can observe the *effects* of processes that occurred before $t_{\rm ls}$. However, any photons that were emitted at proper distances larger than $d_{\rm p}(t_0, z_{\rm ls})$ are very unlikely to reach a present-day observer without having interacted, because they would have been emitted when the Universe was almost completely opaque.

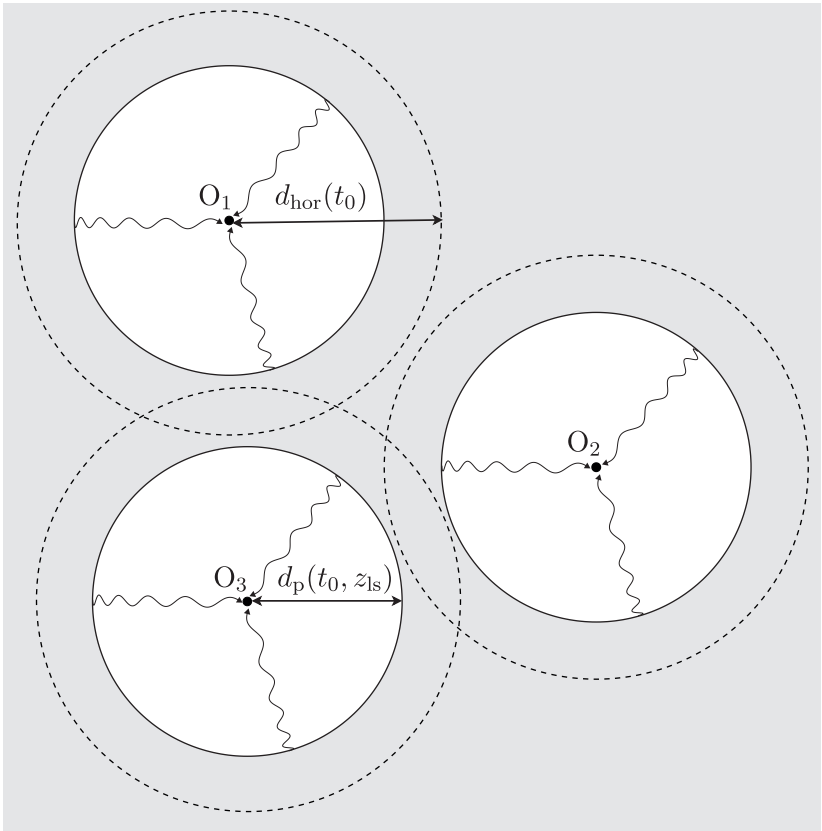

Figure 6.1 Three observers, O_1, O_2 and O_3, at three different, widely separated locations in the Universe at the present cosmic time t_0.

In Figure 6.1, the solid circles represent three different surfaces of last scattering, each having a different observer at its centre. Each surface has the same proper radius $d_{\rm p}(t_0, z_{\rm ls})$, which is equal to the maximum proper distance that photons could have travelled since the epoch of last scattering. The dashed circles represent spherical surfaces with radii equal to the present horizon distance $d_{\rm hor}(t_0)$.

In reality, the Universe's transition from opaque to transparent was not instantaneous. As we will see in the next chapter, different regions of the Universe were slightly denser or hotter than others so all would have become transparent at slightly different times. Accordingly, the last-scattering redshifts of CMB photons span a small range of values centred around $z_{\rm ls}$, such that the 'surface' is actually more like a thin shell.

6.2 Observing the sound of the Universe

In Chapter 1 you saw that maps of the CMB temperature are remarkably uniform but not perfectly smooth. There are tiny differences between the CMB temperatures measured at different locations on the sky. As you continue to work through this chapter, you will learn that one of the primary goals when observing the CMB is to measure the amplitudes of these temperature fluctuations (also commonly referred to as **CMB anisotropies**) and the statistical distribution of their angular sizes. By analysing these measurements, cosmologists can recover a wealth of information about the cosmological parameters and the physical environment of the early Universe.

Fundamentally, the CMB temperature fluctuations reflect a complex pattern of overlapping sound waves with different wavelengths and amplitudes that propagated through the fluids that filled the early Universe. Cosmologists call these sound waves **acoustic oscillations**, and many of the mathematical and statistical techniques that we will use in this chapter have close analogues in the study of acoustics and other wave phenomena. The pattern of temperature fluctuations that we see in the CMB reflects the pattern of acoustic oscillations as it existed at the epoch of last scattering. In the next chapter you will learn much more about the physical processes that govern the detailed properties of the acoustic oscillations and, by extension, the CMB fluctuations.

Before they can derive any cosmological inferences from the CMB, cosmologists must first make detailed observations of its properties. In this section we will review the challenges that are associated with measuring the CMB's properties and the astonishing advances in telescope technology that have made such measurements possible.

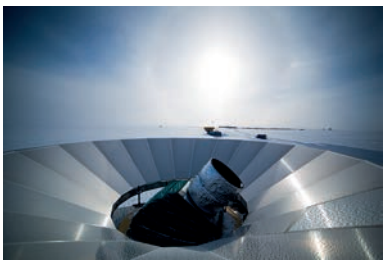

(a)

(b)

(c)

Figure 6.2 The three ground-based microwave telescopes that are currently in operation at the South Pole: (a) BICEP3, (b) the South Pole Telescope, (c) BICEP Array.

6.2.1 CMB observatories and telescopes

As its name suggests, observing the CMB requires telescopes that can detect microwave radiation arriving from space. Observing the CMB from the ground is very challenging because water molecules in the Earth's atmosphere strongly absorb celestial microwaves and can even emit microwave radiation that resembles celestial signals.

To observe the microwave sky from the ground, astronomers must construct their telescopes at high-altitude sites that have very low atmospheric humidity. One location on Earth that fulfils these criteria is the Antarctic Plateau: this region has an average elevation of $\sim 3000\,\mathrm{m}$ and is kept very dry by the extreme cold, which prevents water vapour from forming. Since 1984, several microwave telescopes have been constructed very close to the South Pole; the three currently in operation are shown in Figure 6.2 – BICEP3, the South Pole Telescope and BICEP Array.

Balloon-borne experiments have also been used to observe small areas of the CMB from very high altitude, where the effects of the Earth's atmosphere on the microwave signal are much smaller.

Ultimately, a shared shortcoming of all ground-based and balloon-borne microwave telescopes is that each can only observe a small fraction of the sky. To image the *entire* sky in microwaves using a *single* telescope, the only option is to launch it into space. Figure 6.3 shows examples of the outputs from three space telescopes that have performed all-sky surveys of the CMB with increasing sensitivity and angular resolution.

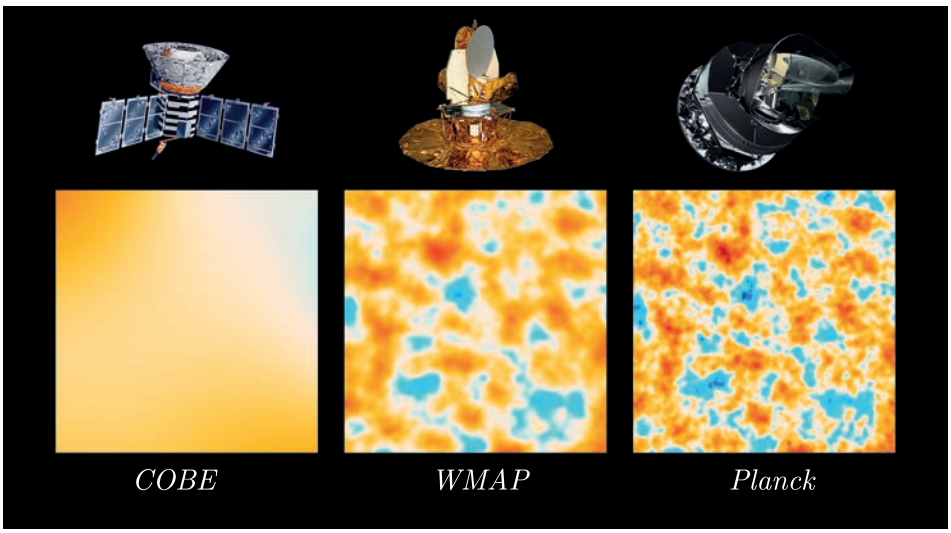

This figure shows relatively small 10-degree-square patches that illustrate the progressive improvement afforded by these different angular resolutions. All three telescopes mapped the entire sky at microwave frequencies.

Figure 6.3 Comparison of the improving angular resolution of three space telescopes that have revolutionised our understanding of the Universe. The *COBE*, *WMAP* and *Planck* satellites produced maps with angular resolutions of 7°, 0.25° and 0.08° (5 arcminutes), respectively.

The first of these missions was NASA's *Cosmic Background Explorer* (*COBE*), which was launched in 1989. *COBE* measured the energy distribution of CMB photons, showing that they follow the perfect black-body spectrum shown in Figure 6.4. The measured black-body temperature enables us to make inferences about the conditions in the early Universe, because the radiation temperature evolved as $T \propto 1 + z$ throughout cosmic history (see Chapter 1).

*C*OBE also provided the first conclusive evidence for the existence of small fluctuations in temperature of CMB photons coming from different directions in the sky.

Janskys

Figure 6.4 plots the intensity of the CMB in units of megajanskys per steradian. The jansky (Jy) is a non-SI unit of spectral flux density that is often used by observational cosmologists and astronomers. In SI units, 1 Jy is equivalent to $10^{-26}\,\mathrm{W\,m^{-2}\,Hz^{-1}}$.

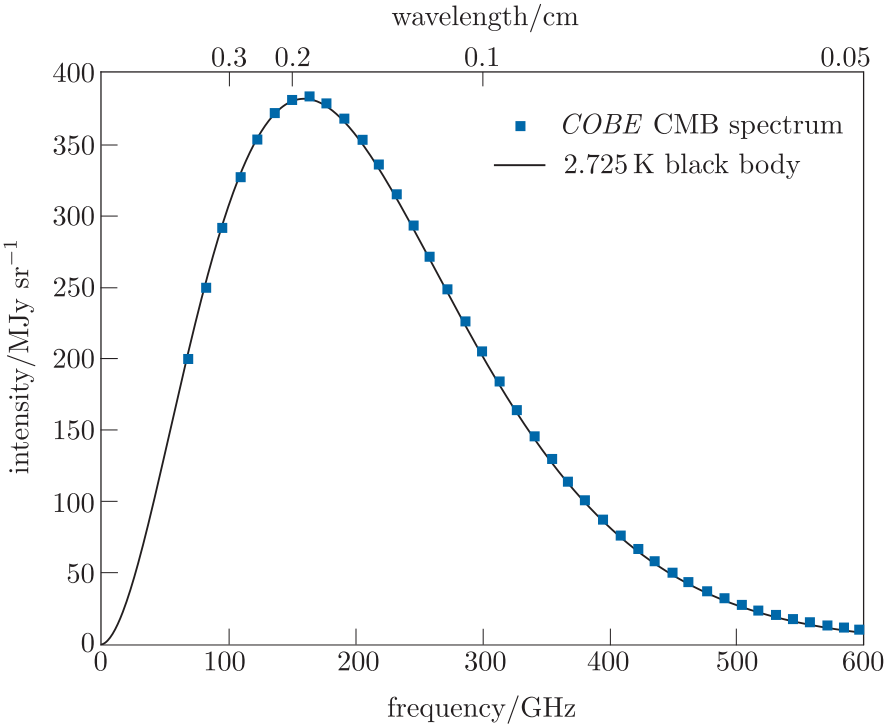

Figure 6.4 The energy spectrum of the CMB as measured by the FIRAS instrument aboard the *COBE* satellite. The curve represents a near-perfect black-body spectrum with a characteristic temperature $T_{\mathrm{CMB}} = 2.725\,\mathrm{K}$.

- In Chapter 1 you learned that this black-body spectrum is characteristic of emission from a medium in perfect thermal equilibrium. What does this equilibrium imply about the contents of the early Universe?
- It implies that at some time in its very early history the entire observable Universe was causally connected and able to exchange energy.

COBE was decommissioned in 1993. It was succeeded in 2001 by NASA's *Wilkinson Microwave Anisotropy Probe* (*WMAP*) and later, in 2009, by the European Space Agency's *Planck* satellite. Both satellites mapped the CMB temperature fluctuations with unprecedented sensitivity and angular resolution. The *Planck* telescope could measure temperature differences as small as one part in a million between patches of sky separated by as little as 5 arcminutes. In the next chapter you will learn how the exquisitely detailed data provided by *WMAP* and *Planck* have allowed cosmologists to derive constraints on the fundamental properties of the Universe.

6.2.2 The noisy microwave sky

Even with sophisticated space telescopes like *WMAP* and *Planck*, making precise measurements of the CMB temperature fluctuations is still difficult. One reason for this is that the CMB is not the only source of microwaves arriving on Earth from space: several other astrophysical processes also emit microwave radiation and can contaminate or obscure the CMB signal. In addition, there are physical phenomena that can distort the observed spectra of CMB photons at different locations on the sky.

The CMB solar dipole

Figure 6.5a shows an all-sky map of the temperature variations in the microwave signal that the *Planck* telescope actually detects. One of the most obvious features of this map is a large-scale temperature gradient called the **CMB solar dipole**.* The pattern of the solar dipole on its own is shown in Figure 6.5b. The solar dipole results from the peculiar motion of the Solar System through space. Fundamentally, it reflects a result from special relativity that observers in different inertial frames will measure different wavelengths for the same photon.

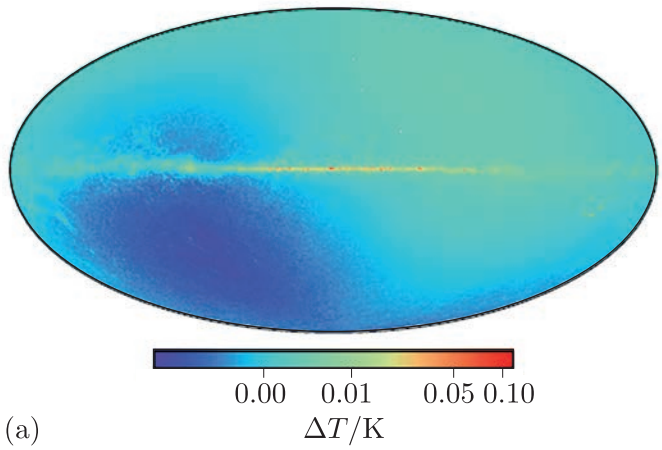

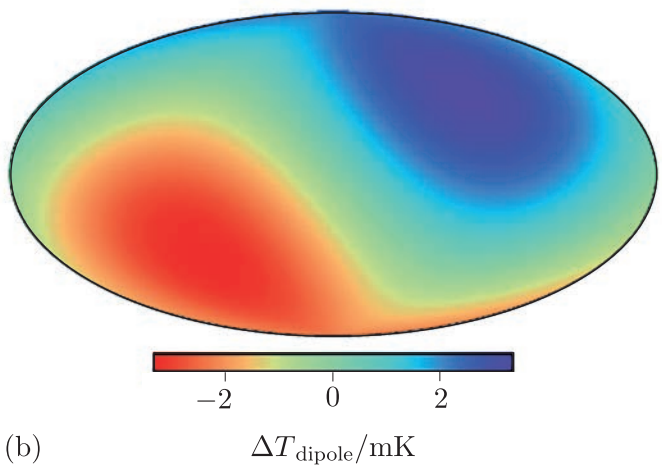

Figure 6.5 (a) An all-sky map of microwave emission coming from space. The CMB solar dipole is clearly visible as large, relatively warm (upper right quadrant) and relatively cool (lower left quadrant) regions. (b) The pattern of temperature variations due to the solar dipole alone.

- Which two inertial frames are relevant when thinking about the origin of the CMB solar dipole?

*The CMB is also modified by another time-varying dipole pattern that is produced by the orbital motion of the Earth around the Sun, but the size of this effect is about 12 times smaller than the solar dipole. The observation strategy of *Planck* is designed so that the signal averages to zero over the course of one year's observations.

○ The first inertial frame is that in which the Solar System is instantaneously at rest. The second frame is one in which the CMB appears isotropic, with no dipole pattern. This is often described as the *CMB rest frame*.

In fact, the first inertial frame is only approximately inertial because the Solar System is being *accelerated* in several directions. Recall that inertial frames move with *constant* velocity with respect to each other. The Solar System is orbiting around the centre of the Milky Way and the Milky Way itself is orbiting around the common centre of mass of the **Local Group** (the gravitationally bound group of galaxies of which the Milky Way is a member). Even the Local Group itself is falling under gravity, towards a local overdensity in the cosmic mass distribution.

In the CMB rest frame, the *present* surface of last scattering is at rest. Remember that observers at different locations in the Universe see different surfaces of last scattering so, because the Earth is moving, the surface of last scattering will change slightly from instant to instant.

In Chapter 2 you learned about the Lorentz transformations, which can be used to convert (or 'map') the four spacetime coordinates from one inertial frame to another. The Lorentz transformations can also be used to show that the motion of the Solar System relative to the CMB rest frame produces a Doppler shift in the frequencies of CMB photons that are observed from Earth or from Earth orbit.

To express this Doppler shift mathematically we need to specify the relative motion of our two inertial frames more formally. We will choose our coordinate axes so that the Solar System rest frame (which we will label as S) and the CMB rest frame (which we will label as S′) are in the 'standard' configuration that you saw in Figure 2.1, with relative velocity V parallel to their common x-axis.

● Does making this specific choice of coordinate axes mean that our Doppler shift expression will not be generally applicable?

○ No. We are only considering two inertial frames, so it is always possible to choose a coordinate system that has its x-axis parallel to the direction of their relative motion.

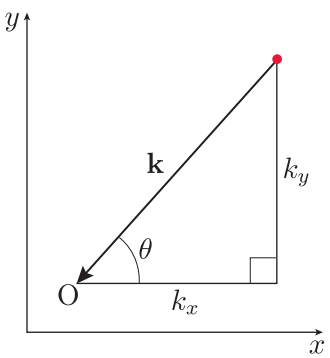

Figure 6.6 An observer at O who is at rest in the inertial frame S detects a photon propagating in the xy-plane. The vector $\mathbf{k}$ defines the direction of the photon's propagation and is shown by the arrow. The photon's trajectory makes an angle θ with the x-axis.

Now consider the scenario shown in Figure 6.6, in which an observer at rest in frame S detects a photon with frequency ν. The vector $\mathbf{k}$, with components k_x and k_y, defines the direction of the photon's propagation in S, and the angle between $\mathbf{k}$ and the x-axis is θ. An observer at rest in S′ will measure a different value ν' for the photon's frequency. If γ is the Lorentz factor corresponding to the relative velocity of S and S′, then ν and ν' are related by the relativistic Doppler-shift formula

$$\nu' = \gamma\nu\left(1 - \frac{V}{c}\cos\theta\right) \tag{6.1}$$

Transforming between S and S′ produces a redshift if k_x is parallel to the relative velocity V of the two frames ($\cos\theta > 0$), and a blueshift if

k_x and V are antiparallel ($\cos\theta < 0$). These frequency shifts preserve the *shape* of the CMB's black-body spectrum but modify its apparent *temperature*. The change in apparent temperature is directly proportional to the change in measured photon frequency, so if T and T' are the CMB temperatures measured in S and S′, respectively, then Equation 6.1 can be rewritten as:

$$T' = \gamma T\left(1 - \frac{V}{c}\cos\theta\right) \tag{6.2}$$

To show that this expression implies the dipole pattern that is observed, we can first assume that the CMB temperature in its rest frame T' is constant in all directions. Now, by replacing γ with its definition in terms of V (Equation 2.5), we can write a series expansion for the *fractional* temperature offset induced by the motion of the Solar System:

$$\begin{aligned}\frac{T}{T'} &= \left(1 - \frac{V^2}{c^2}\right)^{1/2}\left(1 - \frac{V}{c}\cos\theta\right)^{-1} \\ &= \left(1 - \frac{1}{2}\frac{V^2}{c^2} + \cdots\right)\left(1 + \frac{V}{c}\cos\theta + \frac{V^2}{c^2}\cos^2\theta + \cdots\right) \\ &= 1 + \frac{V}{c}\cos\theta + \frac{V^2}{c^2}\left(\cos^2\theta - \frac{1}{2}\right) + \cdots\end{aligned} \tag{6.3}$$

The second term in Equation 6.3 describes the CMB dipole as a *fractional offset* from the mean temperature of the CMB in the rest frame of the surface of last scattering. CMB photons arriving from the direction in which the Solar System is moving are blueshifted and their spectrum appears hotter, while those moving parallel to its motion are redshifted and their spectrum appears cooler. Note that there are also higher-order terms but their impact on the measured CMB temperature turns out to be very strongly suppressed because the Solar System's velocity $V \ll c$.

Example 6.1

The *Planck* satellite measured the amplitude of the solar dipole to be $\Delta T \approx 3.4\,\mathrm{mK}$.

Using this measurement, estimate the speed of the Earth in $\mathrm{km\,s^{-1}}$ relative to the rest frame of the surface of last scattering. You may assume that the *Planck* satellite is at rest in the rest frame of the Solar System and that the Solar System's velocity $V \ll c$. Give your answer to 3 significant figures.

Solution

To solve this problem we will use Equation 6.2. We are told to assume that $V \ll c$, which means that $\gamma \approx 1$. Rearranging gives

$$\frac{T}{T'} \approx \left(1 - \frac{V}{c}\cos\theta\right)^{-1}$$

Now, we are told that ΔT represents the measured amplitude of the solar dipole, and Figure 6.5b shows that the solar dipole pattern is symmetric around $\Delta T = 0$. This means that the measured CMB temperature in the Solar System rest frame varies between $T_{\rm min} = T' - \Delta T$ and $T_{\rm max} = T' + \Delta T$.

Let's consider the maximum in the solar dipole[†], which corresponds with blueshifted CMB photons that are propagating antiparallel to the motion of the solar system, so $\cos\theta = -1$. That means we can rewrite Equation 6.2 as

$$\frac{T_{\rm max}}{T'} = \frac{T' + \Delta T}{T'} \approx \left(1 + \frac{V}{c}\right)^{-1}$$

Now, you learned in Chapter 1 that the mean temperature of the CMB in its rest frame is $T' \approx 2.7\,\mathrm{K}$ and we are told in the question that the dipole amplitude $\Delta T \approx 3.4 \times 10^{-3}\,\mathrm{K}$. Rearranging our previous equation and using these numerical values, we can write:

$$\begin{aligned} V &= c\left(\frac{T'}{T' + \Delta T} - 1\right) \\ &= 3 \times 10^5\,\mathrm{km\,s^{-1}} \times \left(\frac{2.7\,\mathrm{K}}{2.7\,\mathrm{K} + 3.4 \times 10^{-3}\,\mathrm{K}} - 1\right) \\ &= -378\,\mathrm{km\,s^{-1}} \end{aligned}$$

This means that the speed of the Earth relative to the rest frame of the surface of last scattering is $\sim 378\,\mathrm{km\,s^{-1}}$.

- Look again at the short CMB introduction in Chapter 1. How does the amplitude of the solar dipole ($\Delta T \approx 3.4\,\mathrm{mK}$) compare to the maximum amplitude of the CMB temperature fluctuations?
- The maximum amplitude of CMB fluctuations is $\lesssim 300\,\mu\mathrm{K}$ (see the scale provided in Figure 1.9). The solar dipole amplitude is ten times larger than this value.

The variation in observed sky temperature produced by the solar dipole is large enough to significantly distort the observed shapes and amplitudes of the CMB temperature fluctuations. As you will learn later in this chapter, these distortions would effectively prevent accurate inference of the cosmological parameters using CMB observations. Fortunately, cosmologists have developed sophisticated techniques to remove the solar dipole signal from maps of the CMB.

[†]The solar dipole is symmetric so we could also have chosen to consider the solar dipole minimum and we would arrive at the same result.

Astrophysical foreground emission

Figure 6.7 shows the *Planck* skymap after subtracting the solar dipole signal, but before removing the astrophysical microwave foreground. The map shows a bright band of microwave emission coinciding with the Galactic plane, as well as several microwave-emitting, filamentary structures that extend to higher Galactic latitudes.

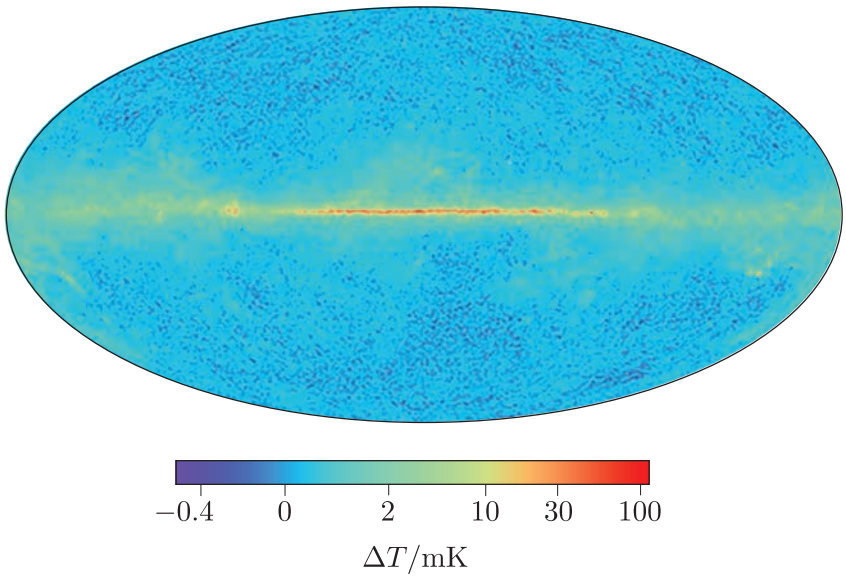

Figure 6.7 *Planck* all-sky map after correcting for the distortion of the solar dipole, but before removing the astrophysical microwave foreground.

Much of this microwave emission comes from radiating particles in the Milky Way. These particles are much closer than the surface of last scattering, so the microwaves they emit are often referred to as 'Galactic foreground' emission. Several physical mechanisms contribute to the Galactic foreground:

- Relativistic electrons emit microwaves via **synchrotron radiation** as they follow spiralling trajectories in the Galaxy's magnetic fields.
- Microwaves in the form of **bremsstrahlung radiation** are emitted when free electrons are accelerated in the Coulomb fields of ions in the **interstellar medium** (ISM). This is commonly known as *free–free emission*.
- Excited molecules in giant molecular clouds and the ISM emit microwaves at specific frequencies as they decay back towards their ground states.
- Interstellar dust grains that rotate at particular frequencies can radiate microwaves if they have a non-zero **electric dipole moment**.
- *Thermal* emission from dust grains at a similar temperature to the CMB is, perhaps unsurprisingly, also in the microwave frequency range.

If the foreground emission were uniform then it would be easy to remove it and reveal the CMB signal. However, the foreground changes by large amounts on different angular scales, which can mask or distort the CMB temperature fluctuations that cosmologists are trying to measure.

Figure 6.8 plots the amount of variation that is produced at different microwave frequencies by the various foreground emission processes and compares this variability with the typical sizes of CMB temperature fluctuations observed by the *Planck* satellite. At almost all frequencies, fluctuations in the combined foreground emission completely dominate those in the CMB signal. The variations are quantified in terms of the **root mean square** (RMS) of the corresponding foreground component's signal around its mean level. The dashed lines show the total RMS temperature variation that is contributed by all the foreground emission processes. At all frequencies except ∼90 GHz this total variation exceeds that of the CMB itself, which is shown by the thin red line.

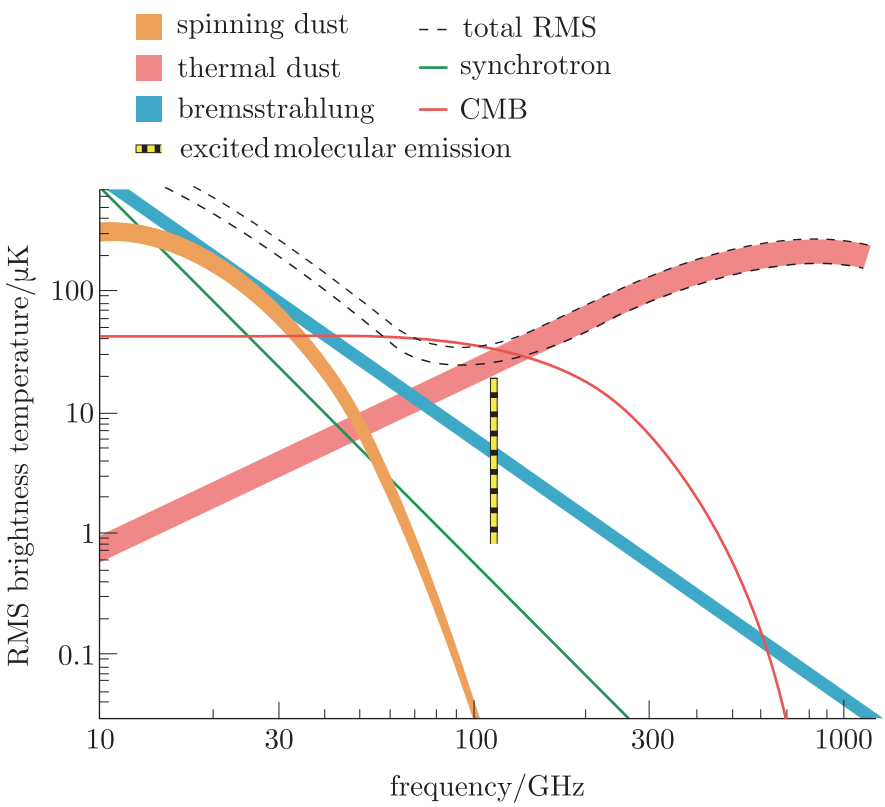

Figure 6.8 The size of *variations* in the measured effective temperature of microwave emission from different components of the diffuse Galactic foreground emission.

Fortunately, cosmologists are able to use observational data and theoretical knowledge about the physical processes involved to build detailed models for the emission from each foreground component as functions of both sky location and photon frequency. By subtracting the combined emission that

is predicted by these models, cosmologists are able to recover the map of the CMB temperature fluctuations shown in Figure 6.9, which is effectively free from foreground contamination.

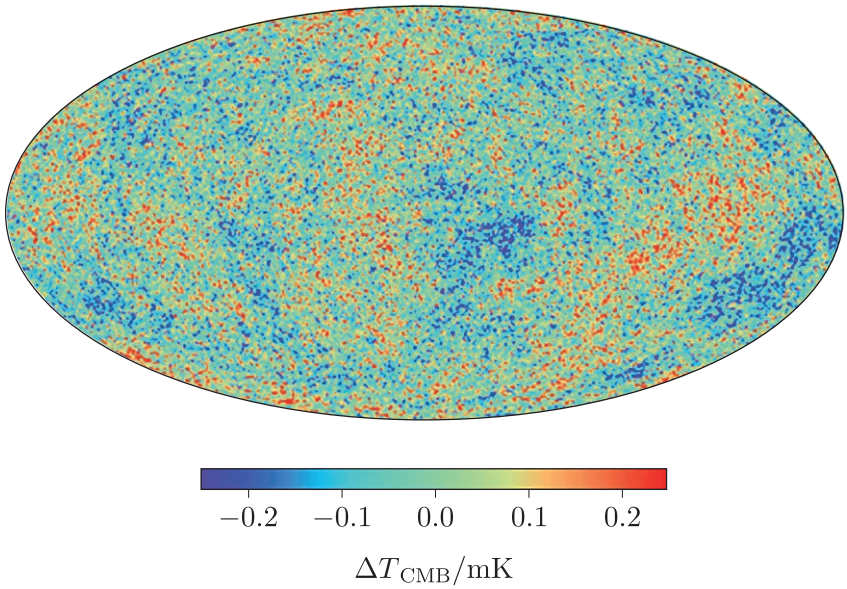

Figure 6.9 The CMB temperature fluctuations after removal of foreground contaminants and the solar dipole. The remaining temperature fluctuations are of the order of hundreds of μK, but they encode a wealth of information about the early Universe and the cosmological parameters.

Next you will read about how cosmologists can mathematically describe and statistically model the pattern of temperature fluctuations shown in Figure 6.9. This mathematical description will allow us to effectively listen to the acoustic oscillations that were introduced in Section 6.2, and, ultimately, to constrain several of the cosmological parameters.

6.3 CMB temperature fluctuations

In this section you will learn more about the CMB temperature fluctuations that were discovered and then probed in detail by the *COBE*, *WMAP* and *Planck* satellites. We will start by constructing a mathematical framework to describe individual temperature fluctuations before introducing the concept of the CMB angular power spectrum, which is a mathematical tool that can be used to examine the amplitudes of sets of fluctuations on different angular scales. In the next chapter you will then learn how various features of the power spectrum arise from processes that were operating during the early Universe, up until the epoch of last scattering.

6.3.1 Describing individual temperature fluctuations

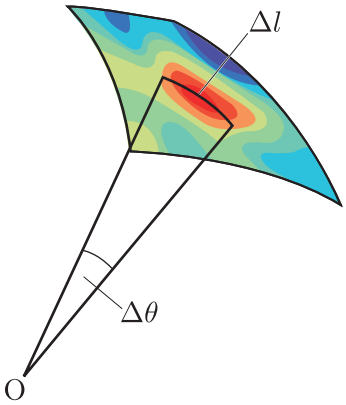

Figure 6.10 An individual CMB temperature fluctuation. An observer at O measures the angular size of the fluctuation to be $\Delta\theta$. Its physical size at the epoch of last scattering is Δl.

For the purposes of this section, let's loosely define an *individual* temperature fluctuation as a contiguous region of the CMB that has a particular observed temperature and is bounded by other regions that have different temperatures.

Before we consider the properties of the CMB as a whole, let's start by exploring two observable properties that can be used to characterise an individual CMB temperature fluctuation like the one shown in Figure 6.10: its *angular size* and its *amplitude*. The angular size $\Delta\theta$ of a temperature fluctuation is interesting because it is related to the physical size Δl of a contiguous region of the Universe at the epoch of last scattering that contained fluids with similar physical properties like density, temperature and velocity.

- Which quantity that you learned about in Chapter 5 relates Δl and $\Delta\theta$ to each other?
- They are related by the angular diameter distance to the surface of last scattering $d_{\mathrm{A}}(z_{\mathrm{ls}})$ such that $\Delta l = d_{\mathrm{A}}(z_{\mathrm{ls}})\,\Delta\theta$.

Let's estimate the physical size of the smallest fluctuations that were resolved by the *Planck* satellite. Their angular size was at the very limit of *Planck*'s angular resolution, $\Delta\theta \approx 5$ arcminutes.

Example 6.2

In Chapter 5 you learned that the present horizon distance $d_{\mathrm{hor}}(t_0)$ is equivalent to the present proper distance that a photon has travelled since the big bang. For the real Universe, it can be shown that $d_{\mathrm{hor}}(t_0) = 14\,165\,\mathrm{Mpc}$.

(a) Using this fact, show that when the redshift of an observed object is very large, such that $z \to \infty$, then a good approximation for its angular diameter distance is

$$d_{\mathrm{A}} \approx \frac{d_{\mathrm{hor}}(t_0)}{z} \tag{6.4}$$

(b) Use this approximation to compute the physical size of the smallest temperature fluctuation that the *Planck* telescope was able to resolve on the surface of last scattering. How does this length scale compare with the physical sizes of objects in the Universe today?

Solution

(a) Because any observable object must be within the particle horizon, the fact that $d_{\mathrm{hor}}(t_0)$ is finite means that the present proper distance to any such object must also remain finite. In fact, it must converge to $d_{\mathrm{hor}}(t_0)$ as the object's redshift $z \to \infty$.

The angular diameter distance is related to the present proper distance by Equation 5.15:

$$d_{\mathrm{A}} = \frac{d_{\mathrm{p}}(t_0)}{1+z} \qquad \text{(Eqn 5.15)}$$

When $z \to \infty$, we can make the approximations that $1 + z \approx z$ and that $d_{\mathrm{p}}(t_0) \approx d_{\mathrm{hor}}(t_0)$, so Equation 5.15 simplifies to the required solution:

$$d_{\mathrm{A}} \approx \frac{d_{\mathrm{hor}}(t_0)}{z}$$

(b) Using Equation 6.4 and the value of $d_{\mathrm{hor}}(t_0) = 14\,165\,\mathrm{Mpc}$ provided in the question, the approximate angular diameter distance to the surface of last scattering is

$$d_{\mathrm{A}}(z_{\mathrm{ls}}) = \frac{d_{\mathrm{hor}}(t_0)}{z_{\mathrm{ls}}} \approx \frac{14\,165\,\mathrm{Mpc}}{1090} \approx 13\,\mathrm{Mpc}$$

This is a remarkably good approximation. Evaluating Equation 5.9 numerically and using the result in Equation 5.15 gives $d_{\mathrm{A}}(z_{\mathrm{ls}}) = 12.77\,\mathrm{Mpc}$.

Using this result we can write an expression for the physical size, l, of a CMB fluctuation on the surface of last scattering that subtends an angle $\Delta\theta$ on the sky today:

$$l = d_{\mathrm{A}}(z_{\mathrm{ls}}) \left(\frac{\Delta\theta}{\mathrm{radians}}\right) \approx 13\,\mathrm{Mpc} \left(\frac{\Delta\theta}{\mathrm{radians}}\right)$$
$$\approx \frac{\pi}{60 \times 180} \times 13\,\mathrm{Mpc} \left(\frac{\Delta\theta}{\mathrm{arcminutes}}\right) \approx 3.8\,\mathrm{kpc} \left(\frac{\Delta\theta}{\mathrm{arcminutes}}\right)$$

Planck was able to resolve angular structures as small as 5 arcminutes. These correspond to regions of the Universe at last scattering with physical proper sizes $\approx$19 kpc. In the present-day Universe, length scales of $\sim$20 kpc are comparable to the physical size of galaxies like the Milky Way.

Exercise 6.1

If the proper size of a region at z_{ls} is 19 kpc, what is its proper size today?

Example 6.3

In Example 6.2 you saw that the angular diameter distance for $z \approx z_{\mathrm{ls}}$ can be well approximated in terms of the current horizon distance $d_{\mathrm{hor}}(t_0)$.

In this short example you will explore a piece of Python code to compute $d_{\mathrm{A}}(z_{\mathrm{ls}})$ directly using Equation 5.15. This will involve first numerically evaluating the integral in Equation 5.9 to find $d_{\mathrm{p}}(t_0)$.

Solution

Please refer to the Example 6.3 Jupyter Notebook in the online module resources to see the solution to this example.

To describe the *amplitude* of CMB temperature fluctuations, cosmologists define a dimensionless quantity that describes the relative difference between the CMB temperature $T(\theta, \phi)$ measured in the direction defined by the angular spherical coordinates θ and ϕ, and the mean CMB temperature $\langle T \rangle$, averaged over the whole sky.

Spherical coordinates were introduced in Chapter 2. Refer to Figure 2.10 if you wish to remind yourself of how they are defined.

The amplitude of CMB temperature fluctuations

$$\frac{\Delta T}{T}(\theta, \phi) \equiv \frac{T(\theta, \phi) - \langle T \rangle}{\langle T \rangle} \tag{6.5}$$

$\langle T \rangle$ can be calculated by evaluating a surface integral:

$$\langle T \rangle = \frac{1}{4\pi} \int_0^{\pi} \int_0^{2\pi} T(\theta, \phi) \sin\theta \, \mathrm{d}\theta \, \mathrm{d}\phi$$

- What is the mean value of $\Delta T/T$ for the whole sky? If $\Delta T/T$ is positive in a particular direction, what does that tell you about the CMB temperature at that location on the sky? What if $\Delta T/T$ is negative?
- By construction, the mean value of $\Delta T/T$ for the whole sky is zero. $\Delta T/T$ will be positive for points on the sky that are warmer than average and negative for points that are cooler than average.

The pattern of temperature fluctuations shown in Figure 6.9 is very complex. It might look like random noise, but in fact it comprises multiple overlapping components with a large range of angular sizes. Cosmologists are interested in the relative prevalence of differently sized fluctuations because this encodes a range of important information about the cosmological parameters and the physics of the early Universe.

To separate out and study sets of fluctuations on different angular scales, it is common practice to expand $\Delta T/T$ into a sum of periodic functions called **spherical harmonics**. The spherical harmonics $Y_{\ell m}(\theta, \phi)$ are two-dimensional functions expressed in terms of the spherical coordinates θ and ϕ that can be used to decompose functions that are defined on the surface of a sphere. Spherical-harmonic expansion is closely analogous to **Fourier expansion**, which can be used to decompose arbitrary functions into a weighted sum of sines and cosines. More detailed background information about spherical harmonics is provided in the next section.

Spherical harmonics

If the integral of the square of a function f between $-\infty$ and $+\infty$ is finite, then f is said to be a square-integrable function. Any square-integrable function $f(\theta, \phi)$ that is defined using spherical coordinates θ, ϕ can be decomposed into an infinite sum of terms:

$$f(\theta,\phi) = \sum_{\ell=0}^{\infty} \sum_{m=-\ell}^{\ell} a_{\ell m} Y_{\ell m}(\theta,\phi) \tag{6.6}$$

The term $a_{\ell m}$ are a set of numerical coefficients that will be explained shortly. The functions $Y_{\ell m}(\theta, \phi)$ are called spherical harmonics and are defined, for integer values of $\ell > 0$ and $-\ell \leq m \leq \ell$, by the expression

$$Y_{\ell m}(\theta,\phi) = \sqrt{\frac{2\ell+1}{4\pi}\frac{(\ell-m)!}{(\ell+m)!}}\, P_\ell^m(\cos\theta)\, \mathrm{e}^{\mathrm{i}m\phi}$$

Figure 6.11 (overleaf) illustrates all the spherical harmonics for which $\ell \leq 3$. Each $Y_{\ell m}$ defines a different two-dimensional, periodic pattern on the surface of a sphere and the values of ℓ and m determine the number of oscillations in the θ- and ϕ-directions, respectively.

In the figure, each oval shows an **Aitoff projection** of the entire surface of a sphere, with the 2π radians around its equator shown in the horizontal (ϕ) direction, and the π radians between its two poles shown in the vertical (θ) direction. Many all-sky maps of the CMB, including the one shown in Figure 6.9, are also drawn using the Aitoff projection. Red and blue colours indicate positive and negative values, respectively. Zero-valued nodes of the $Y_{\ell m}$ function are shown in white.

The dependence of $Y_{\ell m}$ on θ is completely specified by the function $P_\ell^m(\cos\theta)$, which represents an **associated Legendre polynomial**. The integer ℓ is often referred to as the 'multipole number' and, together with m, it determines the number of *nodes* at which $P_\ell^m(\cos\theta) = 0$ between the poles of the sphere, for $-1 < \cos\theta < 1$.

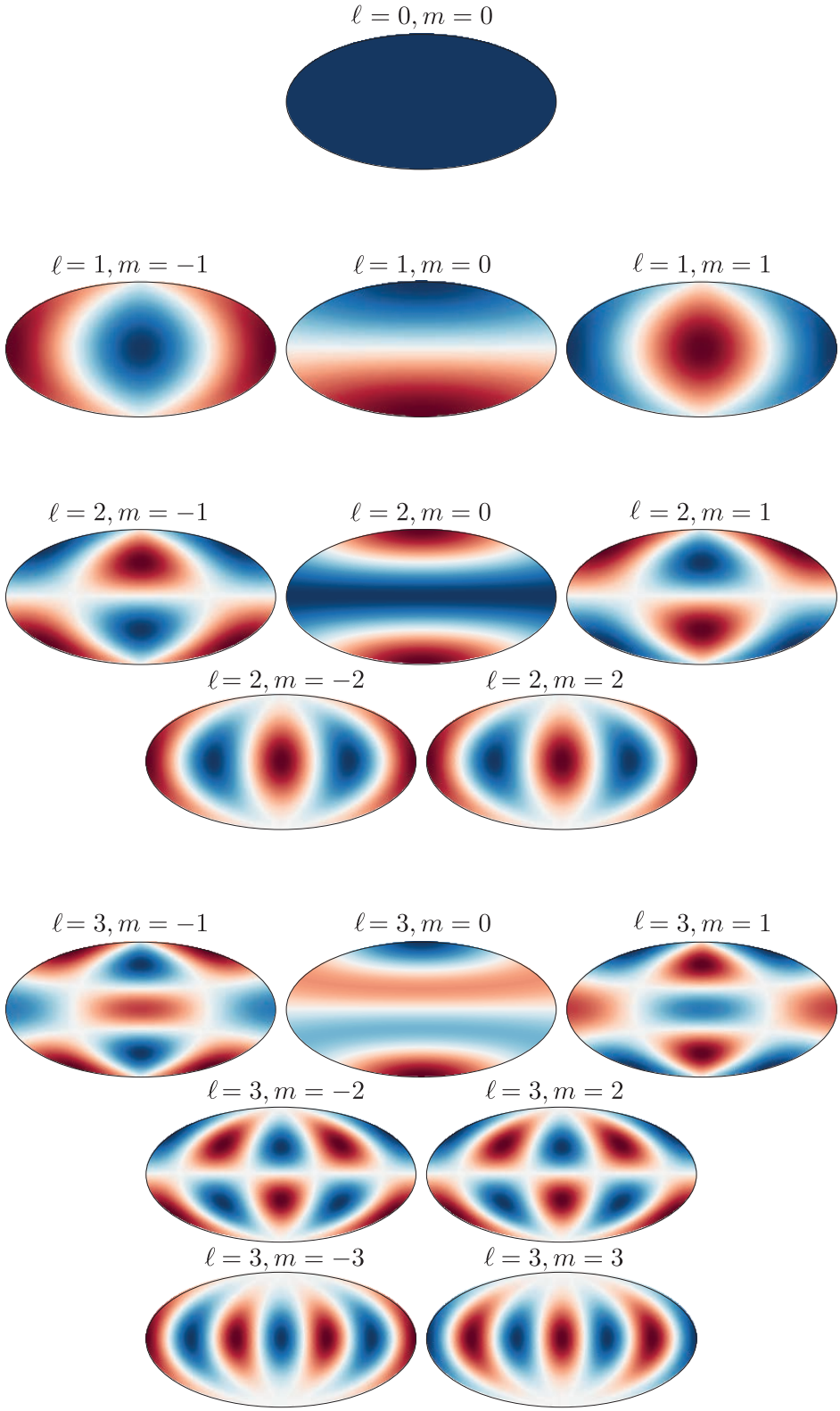

Figure 6.11 An illustration of the real part of the spherical harmonics for $\ell \leq 3$.

Legendre Polynomials

The formula needed to evaluate $P_\ell^m(\cos\theta) = 0$ is a little complicated and we will not quote it here. Instead, Figure 6.12 shows the associated Legendre polynomials for $0 \le \ell \le 5$ and $0 \le m \le 1$ to give an idea of their shapes. For $\ell + m > 1$, the associated Legendre polynomials are oscillatory functions with $\ell - |m|$ *nodes* (where $P_\ell^m = 0$) excluding the end points, and $\ell - |m| + 1$ *extrema* (where $\mathrm{d}P_\ell^m/\mathrm{d}x = 0$) between -1 and 1.

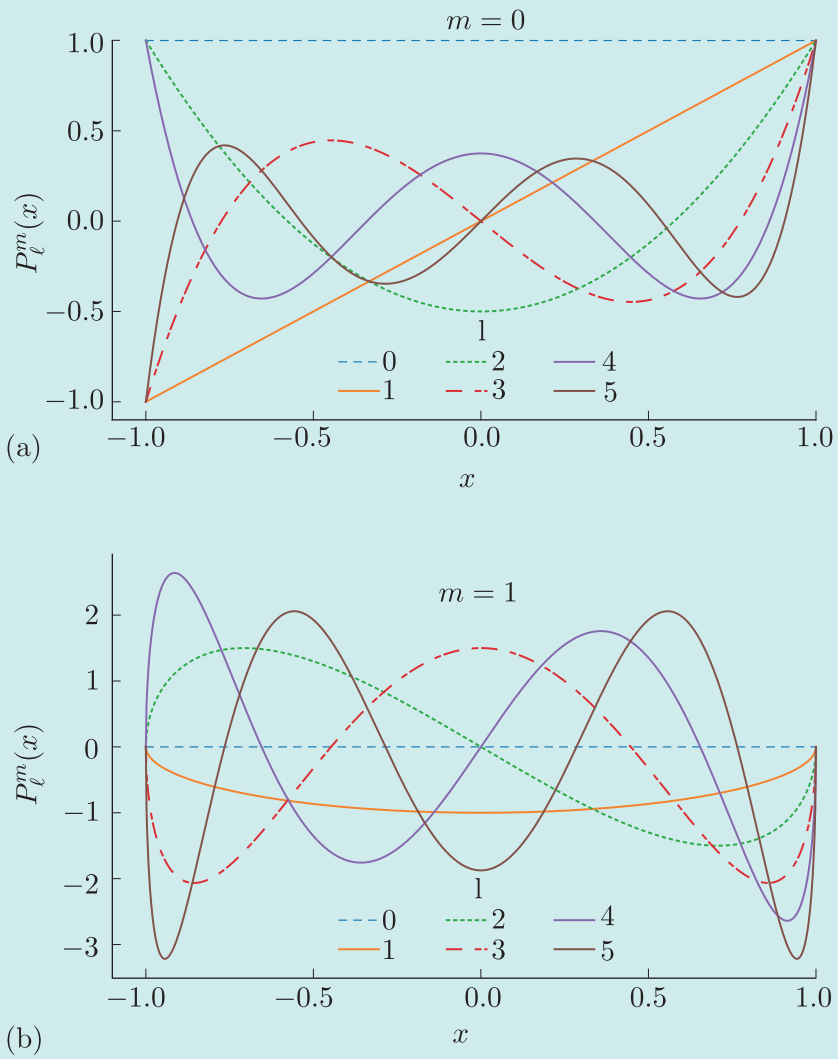

Figure 6.12 The associated Legendre polynomials for $0 \le l \le 5$ and $0 \le m \le 1$.

The azimuthal (ϕ) dependence of $Y_{\ell m}$ is a periodic function, $\mathrm{e}^{\mathrm{i}m\phi}$, that wraps around the circumference of the sphere with $|m|$ complete periods (or, equivalently, $2|m|$ nodes) in the interval $0 \le \phi \le 2\pi$.

The coefficients $a_{\ell m}$ of the spherical harmonics in Equation 6.6 are complex numbers in general, and can be evaluated using

$$a_{\ell m} = \int_{-\pi}^{\pi} \int_{0}^{2\pi} f(\theta, \phi) Y^*_{\ell m}(\theta, \phi) \, \mathrm{d}\Omega$$

where $\mathrm{d}\Omega = \sin\theta \, \mathrm{d}\theta \, \mathrm{d}\phi$ and $Y^*_{\ell m}(\theta, \phi)$ is the complex conjugate of $Y_{\ell m}(\theta, \phi)$.

Having summarised the mathematics of spherical harmonics, we can now use them to write an expansion for the complex pattern of CMB temperature fluctuations as a sum of simpler quasi-periodic functions:

$$\frac{\Delta T}{T}(\theta, \phi) = \sum_{\ell=0}^{\infty} \sum_{m=-\ell}^{\ell} a_{\ell m} Y_{\ell m}(\theta, \phi) \tag{6.7}$$

Individual spherical harmonics are often referred to as *modes* in reference to analogous vibrational modes in acoustics.

Here we have chosen $\Delta T/T$, the observable pattern of temperature fluctuations, to be the function $f(\theta, \phi)$ in Equation 6.6 that we wish to decompose. Each spherical harmonic $Y_{\ell m}$ in the sum represents fluctuations with a particular angular scale ($\Delta\theta \approx \pi/\ell$ radians) and is weighted by an amplitude coefficient $a_{\ell m}$, which carries information about the relative contribution to $\Delta T/T$ from fluctuations on that particular angular scale. The correspondence between ℓ and $\Delta\theta$ is most obvious for the $m = 0$ spherical harmonics illustrated in Figure 6.11, but a closer inspection of the $m \neq 0$ harmonics should convince you that each contiguous region of positive or negative values subtends a solid angle that is characterised by a linear angular scale $\sim\pi/\ell$ radians.

It may help to remind yourself that there are 2π radians around the equator of a sphere, but only π radians between its two poles.

Online resources: exploring the spherical harmonics

The next week-long Python activity, to be studied after completing Chapter 7, will give you the opportunity to explore spherical harmonics in a hands-on way, and learn more about the ways that they can be used to understand the CMB temperature fluctuations.

6.3.2 Statistical descriptions of the CMB

In Chapter 1 you learned that the CMB temperature fluctuations reflect the existence of local inhomogeneities in the matter and radiation density of the Universe at the epoch of last scattering. In later chapters you will learn more about the physical processes that generated these density fluctuations even earlier in the history of the Universe, when $z \gg z_{\mathrm{ls}}$. In this chapter we will not need to understand the fundamental cause of these density perturbations. Instead, we will focus on modelling how they should *evolve* and grow in the time before the epoch of last scattering.

Instead of assuming a *particular* physical origin for the CMB temperature fluctuations, we can model them mathematically as having been generated by a random statistical process. We can then treat the particular pattern of fluctuations that we *do* see as just one possible randomly generated realisation. If we could somehow restart the Universe over and over again,

we would generate a new CMB with a different pattern of temperature fluctuations each time. Even if each new Universe had exactly the same cosmological parameters, the random selection of the initial pattern of density perturbations would still result in a new pattern of temperature fluctuations. Our CMB generator is a random process, so we cannot predict the pattern of temperature fluctuations for any *particular* realisation. However, we *can* predict and write down what the statistical *expectation values* are for different observable properties of the CMB. When cosmologists use theoretical models to predict the statistical properties of the CMB, they are actually predicting these expectation values using different choices for the cosmological parameters.

You can think of the expectation value $\langle X \rangle$ of property X as the average that you would calculate if you measured that property's actual value for an infinite number of different random realisations.

In reality, there is only one CMB that we can observe to measure its properties; our CMB results from one *particular* set of initial density perturbations and it corresponds with the *particular* surface of last scattering that has the Earth at its centre. Observers at different locations in the Universe will observe different CMBs that have a different pattern of temperature fluctuations. Statistically, each of these observed CMBs is a single *sample* from the true pattern of temperature fluctuations that existed throughout the Universe at the epoch of last scattering.

To compare the *observed* properties of our CMB with model predictions, cosmologists need to find some way to estimate those properties' true values using the limited information from the single statistical sample that our particular view of the CMB provides. To do this, they use mathematical functions called **estimators** that can compute theoretical expectation values based on limited statistical samples.

The next section will introduce one of the most important statistical properties of the CMB; you will learn how the theoretical expectation value of this property is defined and how it can be estimated using observational data.

6.3.3 The CMB angular power spectrum

One of the most cosmologically informative properties of the CMB is the variance of $\Delta T/T$, measured on different angular scales. To quantify this variance, cosmologists use a statistical function called the **angular power spectrum**, denoted as C_ℓ.

For a particular value of the multipole number ℓ, the statistical expectation for C_ℓ can be defined as

$$C_\ell \equiv \left\langle |a_{\ell m}|^2 \right\rangle$$

where $|a_{\ell m}|^2 = a_{\ell m} a^*_{\ell m}$ is the squared amplitude associated with a particular $Y_{\ell m}$ in the spherical-harmonic expansion of $\Delta T/T$ (Equation 6.7).

C_ℓ represents a *theoretical* average of $|a_{\ell m}|^2$ over an infinite number of randomly generated CMB realisations for model universes that have identical cosmological parameters.

Recall that for a particular value of ℓ there are only $2\ell + 1$ spherical harmonics $Y_{\ell m}$ and associated amplitudes $a_{\ell m}$ defined for $-\ell \leq m \leq \ell$.

A very important property of C_ℓ is that its value depends only on the angular scale of fluctuations represented by $Y_{\ell m}$ and not on where those fluctuations appear on the sky. Mathematically, this means that for a particular multipole number ℓ, the corresponding amplitudes $a_{\ell m}$ are *statistically independent* and the theoretical expectation value of C_ℓ is identical for all permitted values of m.

We can use this fact to derive an estimator for the angular power spectrum. The sample of $|a_{\ell m}|^2$ values we observe is unlikely to equal the corresponding set of expected values because of the inherently random nature of the way the CMB temperature fluctuations were produced. However, once we have expanded $\Delta T/T$ using spherical harmonics, we will have $2\ell + 1$ *measured* $a_{\ell m}$ values for each value of ℓ. Then, for each value of ℓ, we can use the mean of the squares of all the corresponding measured amplitude values as an estimator, $\widehat{C_\ell}$, for the true value of the power spectrum:

We use the hat notation $\widehat{C_\ell}$ here to indicate a statistical estimate for the unknown true value of the quantity C_ℓ.

$$\widehat{C_\ell} = \frac{1}{2\ell + 1} \sum_{m=-\ell}^{\ell} |a_{\ell m}|^2 \tag{6.8}$$

Cosmic variance

Intuitively, we might expect that averaging together more measurements of $|a_{\ell m}|^2$ would result in a more accurate estimate, and that is indeed the case. However, no matter how carefully we measure the angular structure of the CMB we observe, the values of $\widehat{C_\ell}$ that we calculate can never be perfectly accurate estimates of the true values of C_ℓ. Based on fundamental statistical theory, the expected variance of our estimated $\widehat{C_\ell}$ values around the true values of C_ℓ is

$$\sigma^2(\widehat{C}_\ell, \ell) = \frac{2}{2\ell + 1} \widehat{C_\ell}^{\,2} \tag{6.9}$$

Equation 6.9 represents an irreducible uncertainty in our measurements of the power spectrum, which cosmologists call **cosmic variance**. It reflects the fact that observing from a single location in the Universe provides incomplete information about the underlying distribution of temperature fluctuations that are only *sampled* by the CMB. Cosmic variance is particularly relevant on large angular scales, which correspond to small values of ℓ and therefore have fewer independent $|a_{\ell m}|^2$ values to average.

From theory to observation

Figure 6.13 presents the CMB angular power spectrum measured by the *Planck* satellite. Instead of plotting C_ℓ directly, it is conventional to use a scaled quantity that has units of squared temperature:

$$\Delta_T^2 = \frac{\ell(\ell + 1)}{2\pi} C_\ell \langle T \rangle^2 \tag{6.10}$$

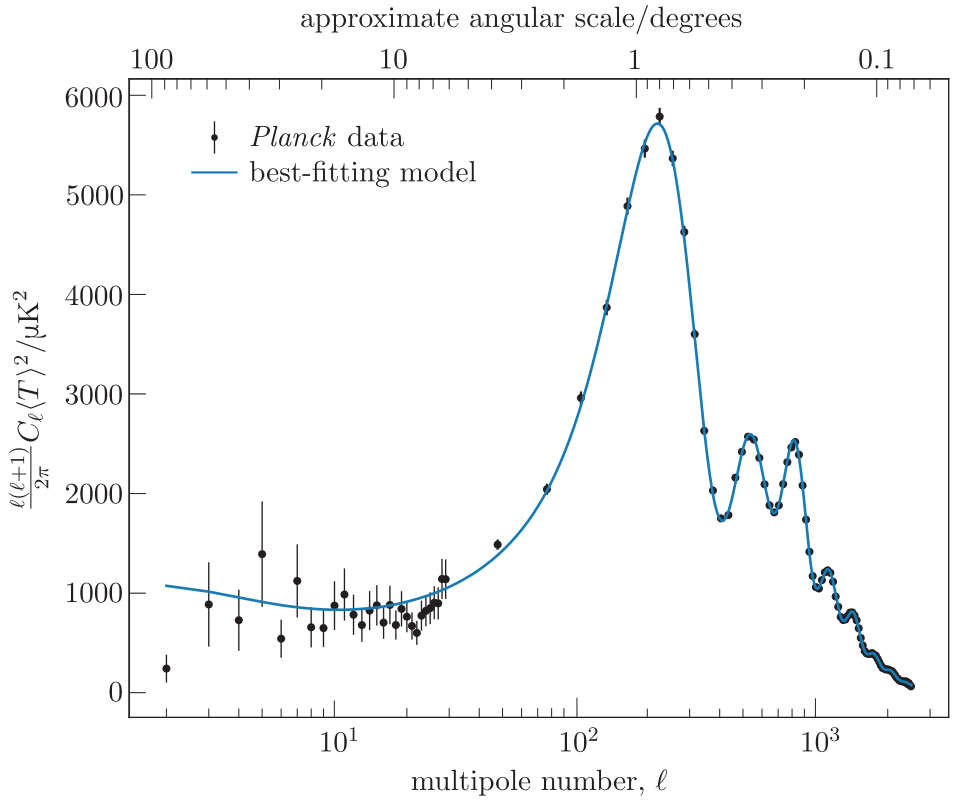

Figure 6.13 The CMB angular power spectrum measured by the *Planck* satellite. The black points show the measurements and the vertical bars show the associated errors.

Note how the effect of cosmic variance increases the scatter on large angular scales (bottom left of figure). The blue line shows the theoretical model that best fits the observed data. The normalisation factor of $\ell(\ell+1)/2\pi$ in Δ_T^2 is a historical convention. It has the useful property that a graph of Δ_T^2 versus ℓ would be approximately flat *if* the variance of the *density* fluctuations that imprinted their distribution on the CMB was equal on all *physical* scales.

Figure 6.13 shows us that the *observed* spectrum of Δ_T^2 is definitely *not* flat except at very low values of ℓ. It contains several obvious peaks and even the narrow 'plateau' that appears for $\ell \lesssim 20$ is not perfectly level. However, this complicated structure in the observed CMB angular power spectrum does not necessarily mean that the *primordial* density fluctuations did not have equal variance on all physical scales, only that this was no longer true by the time of last scattering. If the earliest density perturbations had equal variance on all physical scales, then the observed angular power spectrum tells us that the power spectrum of those initial perturbations was modified by physical processes that operated during the early history of the Universe when $z > z_{\rm ls}$. In the next chapter you will learn what these processes were, how they depend on the values of various cosmological parameters and how we can use the observed power spectrum to constrain what the values of those cosmological parameters are.

6.4 Summary of Chapter 6

- For the first $\sim 370\,000$ years of its history, the baryonic content of the Universe existed as an almost completely ionised plasma. During this time, the Universe was opaque to photons, which could only travel short distances before scattering from free electrons in the plasma.
- The Universe became transparent to photons during a short time interval that ended at the **epoch of last scattering**. The cosmic microwave background (CMB) comprises photons that were released during this interval and have propagated without scattering ever since.
- The CMB photons that we observe today have all travelled very similar distances to reach the Earth. This means that they can be considered to come from a **surface of last scattering** at a redshift $z \approx 1090$.
- The energy spectrum of the CMB photons follows a perfect black-body distribution, which is strong evidence that the whole Universe was in thermal equilibrium very early in its history.
- The radiation temperature of the Universe (and hence the black-body temperature of the CMB) evolved since the epoch of last scattering according to $T \propto 1 + z$.
- The black-body temperature of the CMB spectrum $T(\theta, \phi)$, measured at different points on the sky, exhibits tiny variations with amplitudes $\lesssim 300\,\mu\text{K}$ around a mean value of $\langle T \rangle = 2.725\,\text{K}$. These variations are called CMB temperature fluctuations and they are expressed mathematically as

$$\frac{\Delta T}{T}(\theta, \phi) \equiv \frac{T(\theta, \phi) - \langle T \rangle}{\langle T \rangle} \qquad \text{(Eqn 6.5)}$$

- The complex pattern of fluctuations reflects density perturbations that were present in the Universe at the epoch of last scattering. These density perturbations were produced by an ensemble of overlapping sound waves that were propagating through the fluids filling the early Universe. These sound waves are called **acoustic oscillations**.
- Cosmologists decompose the complex two-dimensional pattern of temperature fluctuations into a series of simpler, periodic, two-dimensional functions $Y_{\ell m}(\theta, \phi)$ called **spherical harmonics**, each of which describes fluctuations on a specific angular scale:

$$\frac{\Delta T}{T}(\theta, \phi) = \sum_{\ell=0}^{\infty} \sum_{m=-\ell}^{\ell} a_{\ell m} Y_{\ell m}(\theta, \phi) \qquad \text{(Eqn 6.7)}$$

- The CMB **angular power spectrum** $C_\ell(\ell)$ measures the contribution of fluctuations on a particular angular scale to the overall variance of the CMB temperature. The spectrum exhibits several peaks, indicating larger contributions to the variance by fluctuations on specific angular scales.

- The coefficients $a_{\ell m}$ in the spherical-harmonic decomposition of the *measured* CMB temperature fluctuations can be used to *estimate* the CMB angular power spectrum:

$$\widehat{C_\ell}(\ell) = \frac{1}{2\ell+1} \sum_{m=-\ell}^{\ell} |a_{\ell m}|^2 \qquad \text{(Eqn 6.8)}$$

- The inherent uncertainty associated with measuring $\widehat{C_\ell}(\ell)$ based on the CMB spectrum observed from just one location (Earth) is known as **cosmic variance**.